Biotransformation of bisphenol-A bis(diphenyl phosphate): *In vitro, in silico*, and (non-) target analysis for metabolites in rat and bird liver microsomal models

Sofia M. Herczegh[a,b], Shaogang Chu[a], Robert J. Letcher[a,b*]

[a] Ecotoxicology and Wildlife Health Division, Environment and Climate Change Canada, National Wildlife Research Centre, Carleton University, Ottawa, ON, K1A 0H3, Canada

[b] Department of Chemistry, Carleton University, Ottawa, ON, K1S 5B6, Canada

* Corresponding author: Robert J. Letcher; Phone: 1-613-998-6696; Fax: 1-613-998-0458; E-mail: robert.letcher@ec.gc.ca.

Highlights

- 44% bisphenol-A bis(diphenyl phosphate) (BPADP) *in vitro* was depleted in rat assays
- In rat assays 2.6% and 3.9% of BPADP was converted to DPHP and BPA, respectively
- No significant BPADP depletion or BPA and DPHP formation in herring gull assays
- *In silico* estimation of metabolites BPA and DPHP confirmed by rat and gull assays
- Other BPADP oxidation metabolites and conjugate identified by non-target screening

Graphic Abstract

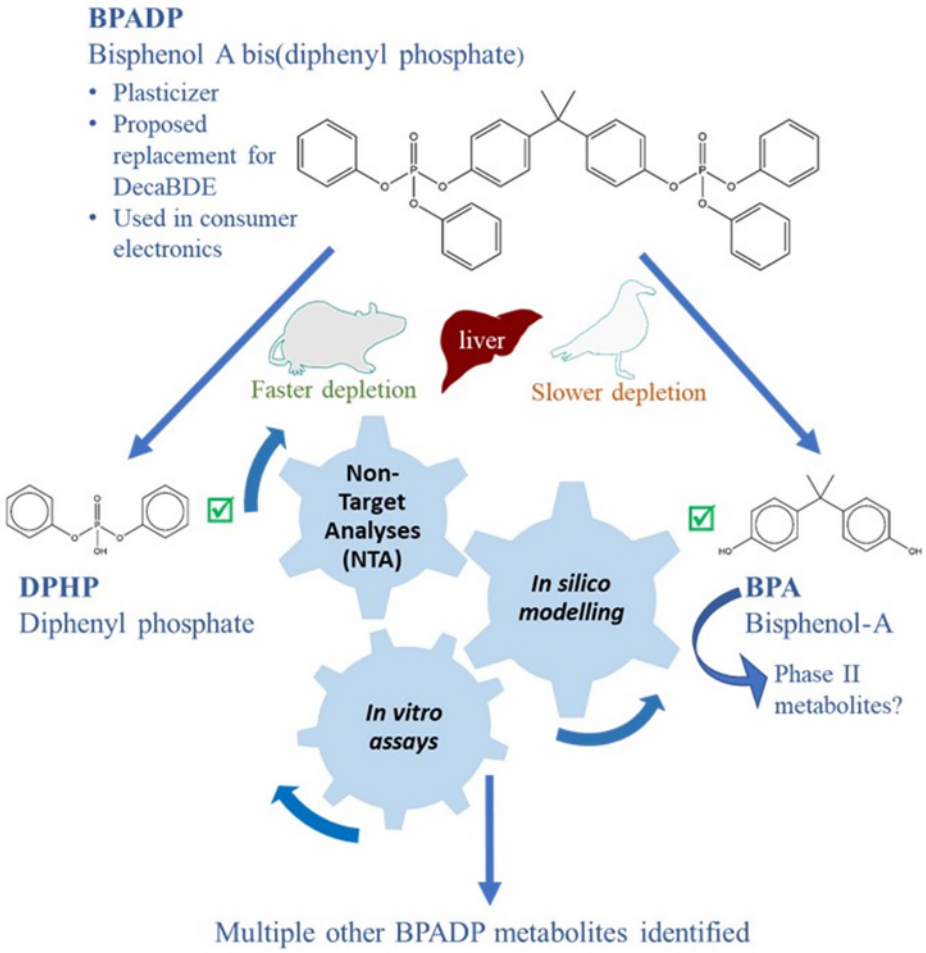

Abstract

Increased production and usage of organophosphate esters (OPEs) as flame retardants and plasticizers has trended towards larger and 'novel' (oligomeric) OPEs, although there is a dearth of understanding of the environmental fate, stability, toxicokinetics, biotransformation and bioaccumulation of novel OPEs in exposed biota. The present study characterized *in vitro* biotransformation of the novel OPE bisphenol-A bis(diphenyl phosphate) (BPADP) using Wistar-Han rat and herring gull liver based microsomal assays. Hypothesized target metabolites bisphenol-A (BPA) and diphenyl phosphate (DPHP) and other metabolites were investigated by applying a lines of evidence approach. *In silico* modelling predicted both BPA and DPHP as rat metabolites of BPADP, these metabolites were quantified via UHPLC-QQQ-MS/MS. Additional non-target metabolites were determined by UHPLC-Q-Exactive-Orbitrap-HRMS/MS and identified by Compound Discoverer software. Mean BPADP depletion of 44 ± 10% was quantified with 3.9% and 2.6% conversion to BPA and DPHP, respectively, in the rat assay. BPADP metabolism was much slower when compared to the well-studied OPE, triphenyl phosphate (TPHP). BPADP depletion in gull liver assays was far slower relative to the rat. Additional non-target metabolites identified included two Phase I, O-dealkylation products, five Phase I oxidation products and one Phase II glutathione adduct, demonstrating agreement between lines of *in vitro* and *in silico* evidence. Lines of evidence suggest that BPADP is biologically persistent in exposed mammals or birds. These findings add to the understanding of BPADP stability and biotransformation, and perhaps of other novel OPEs, which are factors highly applicable to hazard assessments of exposure, persistence and bioaccumulation in biota.

***Keywords*:** Organophosphate esters, Biotransformation and metabolism, *In silico*, *In vitro*, bird and rat models, non-target analysis

1. Introduction

Flame retardant (FR) chemicals, used in a variety of consumer products as both plasticizers and FRs, consist of a variety of compounds categorized by chemical properties and structure (van der Veen and de Boer, 2012; NIEHS, 2018; Yao et al., 2021). Brominated FRs (BFRs) include polybrominated diphenyl ethers (PBDE) technical formulations (pentaBDE, octaBDE and decaBDE) comprised of varying congeners, which were produced and used extensively before largely being replaced by organophosphate ester FRs (OPEs) (van der Veen and de Boer, 2012; Blum et al., 2019). Following strong evidence of the persistent, bioaccumulative and toxic (PBT) nature of PBDEs, pentaBDE and octaBDE were listed under Annex A (elimination) of the Stockholm Convention on persistent organic pollutants (SC-POPs) in 2009 and decaBDE was listed in 2017 (UNEP, 2019).

Bisphenol-A bis(diphenyl phosphate) (BPADP; CAS RN 5945-33-5) is an OPE proposed as a replacement for decaBDE (Rossi and Heine, 2007). In 2006, the production volume of BPADP in the United States was estimated to be within the range of 4500-23000 tons (van der Krowech et al., 2016; Veen and de Boer, 2012). Similar to the majority of OPEs, BPADP is an additive FR compound, posing a higher risk of entering the environment compared to reactive and chemically-bonded FRs (Velencoso et al., 2018). Based on physico-chemical properties and limited available literature concerning the compound, BPADP could be considered a ‘novel’, oligomeric OPE along with other OPEs such as resorcinol bis(diphenylphosphate (RDP) and tetrakis(2,6-dimethylphenyl)-m-phenylene biphosphate (RDX). As industry trends move towards polymerization and longer-chain, larger replacement FRs such as BPADP, more study is needed concerning the fate, transformation and effects of such compounds.

Considering physico-chemical properties and environmental behaviour of BPADP, an experimentally derived logK_{OW} value for BPADP was '≥6' (ECHA, 2011) and logK_{OC} values of 4.00 ± 0.473 and 4.76 ± 0.252 were reported for water – suspended particulate matter (SPM) and water – sediment, respectively (Zhong et al., 2021). Such coefficients suggest lipophilicity and high affinity to sediment, with bioaccumulation factors (BAF) of $4.0e^3$ L water/g lipid ($4.0e^6$ L water/kg lipid) and $1.3e^2$ to $2.1e^2$ L water/g lipid ($1.3e^5$ to $2.1e^5$ L water /kg lipid) for plankton and fish, respectively, reported in a study of Taihu Lake, China (Zhao et al., 2019).

Bekele et al. (2021) concluded that only a few studies have reported on the metabolic transformation of OPEs *in vitro* in cells or microsomes, and even fewer studies have shown metabolism of OPEs *in vivo*. These studies are limited to six "legacy" OPEs including TPHP. Cytochrome P450 (CYP450) enzymes have been found to mediate the metabolism of several OPEs (e.g. TPHP, tris(2-chloroethyl) phosphate (TCEP), tris(1-chloro-2-propyl) phosphate (TCIPP), tris(1,3-dichloro-2-propyl) phosphate (TDCIPP)), and require nicotinamide adenine dinucleotide phosphate (NADPH) (van den Eede et al., 2013). However, a preliminary study of BPADP human liver microsomal (HLM) and S9 fraction metabolism suggested NADPH-independent enzymes may play an important role in the metabolism of BPADP (Alves et al., 2018). An example may be paraoxonase (PON) enzymes, specifically paraoxonase 1 (PON1), which has been found to exhibit high efficiency in catalyzing the metabolism of the particular organophosphates diazoxon and chlorpyrifos oxon (Draganov and La Du, 2003).

The metabolic pathways of O-dealkylation, abiotic hydrolysis, glucuronidation and sulfation appear to be relevant for BPADP (Alves et al., 2018). BPADP may degrade into BPA, a plastic additive, estrogen-mimicking compound (Rubin, 2011) and aquatic toxicant (Wu and Seebacher, 2020). In the present study, a lines of evidence approach informed on BPADP

biotransformation and environmental fate, combining *in silico* modelling, *in vitro* inter-species biotransformation using target metabolite identification and non-target analysis for possible additional metabolites.

2. Materials and methods

2.1 In silico metabolite profiling

Prior to *in vitro* microsomal assays, rat liver S9 and microsomal metabolites as well as rat *in vivo* metabolites were simulated using the publicly available OECD Toolbox v4.4.1 (OECD, 2021) (Paris, France). Predicted metabolites were generated in ranked order of probability of occurrence, displayed via unique Simplified Molecular Input Line Entry System (SMILES) code (Table S-1). A test of the OECD Toolbox was performed using the model OPE, TPHP, for which target metabolites from an *in vitro* rat assay have been identified (Chu and Letcher, 2019) to verify the utility of the model for identification of both Phase I and II metabolism reactions relevant to OPEs. BPADP was further screened through EPI Suite^{TM} v4.1.1 (US EPA, 2012) for environmental fate predictions. Model training sets were reviewed with certain models excluded given the high molecular weight and low water solubility of BPADP.

2.2 Chemicals and reagents

BPADP standard (98 %) was obtained from Toronto Research Chemicals (Toronto, ON, CA) and a spiking solution was prepared by dissolving BPADP in dimethyl sulfoxide (DMSO). Internal standards d_{15}-TPHP (> 98 % purity), and d_{10}-DPHP (95 % purity), were obtained from Wellington Laboratories (Guelph, ON, Canada) and Toronto Research Chemicals (Toronto, ON, Canada), respectively. BPA, DPHP and TPHP (each > 99+ % purity), as well as the internal standards $^{13}C_{12}$-BPA (> 98 % purity) and trans-1,4-cyclohexanediol bis(diphenyl phosphate) (TCHBDP; > 97 % purity) were obtained from Sigma-Aldrich (St. Louis, MI, USA). Gentest

Male Wistar-Han rat liver microsomes (20 mg/mL protein), and NADPH regenerating system solutions A (NADP+ and Glc-6-PO_4) and B (G6PDH) were obtained from Corning Inc. (Corning, NY, USA). All glassware were cleaned at 450 ^oC overnight prior to each assay to reduce possible OPE contamination.

Rat and gull liver microsomes and NADPH system solutions were stored at -80 ^oC, with aliquots thawed on ice for the assays. Deactivated microsomes were prepared by heating of microsomes to 100 °C for 5 min in a water bath and then stored in freezer (-80 °C) until further use. Potassium phosphate buffer (0.5 M; pH=7.4) was purchased from Alfa Aesar (Ward Hill, MA, USA). L-Glutathione reduced (≥ 98 % purity) was obtained from Sigma-Aldrich in powdered form. A complete list of referenced compounds is provided in Table S-2.

2.3 In vitro liver microsomal assay optimization for BPADP

BPADP metabolism kinetics were investigated to determine the concentration of BPADP that achieves enzyme substrate saturation (zero-order kinetics) and maximum biotransformation rate ([BPADP] >> 2(K_M)). A kinetics assay was designed based on previous findings that enzyme system saturation is achieved at a final dosing concentration of 2 µM (Greaves et al., 2016; Strobel et al., 2018), therefore, initial depletion of BPADP and formation of DPHP were quantified in a 10 minute incubation with aliquots taken at t_0, t_2, t_5 and t_{10}. Kinetics assays were conducted at a range of five BPADP incubation concentrations between 0.514 µM and 2.57 µM.

The day prior to each assay, a BPADP spiking solution was prepared in potassium phosphate buffer (50 mM, pH 7.4) and deionized water then sonicated in an amber bottle and then sonicated in a sonication bath for 24 hours to increase BPADP bioavailable within the aqueous assay given its low water solubility and high molecular mass.

Triplicate biotransformation assays were conducted at BPADP incubation concentrations of 1780 ppb (or 2.57 µM), with each active, blank and control test tube (each at total volumes of 950 µL) shaken at 80 rpm and 37 ^{o}C for 2 minutes minimum. Addition of 50 µL of microsomal suspension (either Wistar-Han rat or herring gull) to the respective incubation tube (total volume 1 mL) initiated the reaction. All biotransformation incubations were vortexed for 20 seconds to allow for homogenization (TPHP positive control vortexed for 5 seconds due to known rapid metabolism), and a 100 µL aliquot was taken within 30 seconds of reaction initiation. Aliquots from the biotransformation assay were also taken at the 5, 10, 20, 40, 60, 90 and 120- min time points, with a 2 min time point aliquot additionally taken for TPHP positive controls. To terminate each reaction, aliquots were added to the appropriate time point test tube containing 300 µL acetonitrile (ACN) and 100 µL of 40 ppb combined internal standard for a total volume of 500 µL. All samples were filtered through pre-rinsed VWR Modified Nylon 0.2 µm, 500 µL centrifugal filters, centrifuged at 10 000 rpm for 5 minutes and transferred to UHPLC vials for analysis.

A modified *in vitro* rat liver microsomal (RLM) assay was conducted to generate samples suitable for Target and non-target analysis (NTA) by UHPLC-Q-Exactive-HRMS/MS for screening of additional BPADP metabolites. Reactions were terminated by addition of 4 mL diethyl ether, centrifuged at 3500 rpm for five minutes, frozen for a minimum of one hour before retention of ether phase, then volatilized with 100 µL UHPLC-grade methanol added to dried sample. All samples were sonicated for 10 minutes and filtered through pre-rinsed PALL Life Sciences Nanosep 0.2 µm wwPTFE centrifuge filters for five minutes at 3500 rpm then transferred to vials for UHPLC-Q-Exactive-HRMS/MS analysis. Following the findings of Chu and Letcher (2019), 0.15 g/mL GSH solution was prepared in deionized water immediately prior

to the experiment for investigation of potential BPADP adducts with GSH. Method blanks of the modified assay for NTA were prepared at an equivalent total incubation volume and therefore used as non-GSH controls.

2.4 UHPLC-QQQ-MS/MS analysis

Analysis of time-dependent *in vitro* biotransformation assay samples was conducted utilizing Waters Acquity Ultra High Performance Liquid Chromatography coupled to a Waters Xevo TQ-S Triple Quadrupole Mass Spectrometer (UHPLC-QQQ-MS/MS) operated with an electrospray ionization (ESI) source. The method used in the present study was based on our previous methods with some modifications (Chu and Letcher, 2015, 2018; Su et al., 2015b). A Kinetex EVO C18 column (50 x 2.1 mm, 1.7 μm particle size) was used to separated analytes. Column and sample temperature were 45 °C and 20 °C, respectively. The mobile phases were water (A) and methanol (B) and both contained 2 mM ammonium acetate, and the injection volume was 10 μL. The initial flow rate was set to 0.5 mL/min, mobile phase B starting at 5 % and the gradient increasing for five minutes to 95 % mobile phase B, held for five minutes and concluding at a total 15 minute run time. The MS/MS was operated in both ESI+ and ESI- modes. During 1 to 4.2 min MS/MS operated in negative mode, after that it switched to positive mode. The nebulizing gas was nitrogen and argon was used as the collision gas. The capillary voltage was 2.5 kV, and source and desolvation temperatures were 150 °C and 500 °C, respectively. The desolvation gas flow rate was 1000 L/hr and the cone gas flow rate 150 L/hr. MS/MS analysis was performed using the multiple reaction monitoring (MRM) mode and six functions are set in the MS method. The MRM transitions, compound dependent operation parameters, and retention times are listed in Table S-3.

After UHPLC-Q-Exactive HRMS/MS analysis of the assay fractions (see next section, 2.5) and using an alternate UHPLC-QQQ-MS/MS analytical method, additional metabolite targeting and re-analysis occurred for *in vitro* triplicate samples, method blanks, enzymatically deactivated and NADPH deficient controls samples. In this alternate UHPLC-QQQ-MS/MS analytical method the operation parameters were the same as described for the initial method except that the MS/MS was operated in ESI(+) mode for monitoring transitions of the four additional targeted metabolites, i.e. BPA-DPP, BPA-DPP-MPP, BPADP+O and BPADP+2O (Table S-3).

UHPLC-QQQ-MS/MS sample analysis and MassLynx v4.1 software (Waters, 2014) quantified the initial target BPADP depletion and BPA and DPHP metabolite formation with back calculation to represent assay incubation concentrations. An 8-point calibration curve was quantified between every 16 samples to ensure linearity of response, with the calibration standards prepared to have metabolite concentrations 1/5 of the BPADP concentration and a constant combined internal standard concentration to account for low metabolite formation. For the additional four target metabolites (Table S-4), quantification was not possible due to the lack of suitable internal standards. Thus, the relative concentration change of these analytes was determined by UHPLC-QQQ-MS/MS peak response over time.

2.5 UHPLC-Q-Exactive-HRMS/MS analysis

Target analysis and non-target analysis (NTA) for identification of additional metabolites and GSH adducts was via a Vanquish UHPLC coupled with a quadrupole orbitrap mass spectrometer (UHPLC-Q-Exactive-HRMS/MS; ThermoScientific, Waltham, MA, USA). Details of all these analyses are fully described in the Supplemental Information.

Target and non-target metabolite screening and identification following UHPLC-Q-Exactive-HRMS/MS *in vitro* sample fraction analysis was conducted using the automatic search

capabilities of Compound Discoverer version 3.2 (ThermoFisher Scientific, Waltham, MA, USA) and included automatic blank subtraction with the following transformations searched: Phase I, dearylation, dehydration, demethylation, desaturation, hydration, oxidation, reduction, ionization and loss of a diphenyl phosphate group. For GSH adduction search the transformation search also included Phase II GSH conjugation 1(->$C_{10}H_{15}N_3O_6S$) and GSH conjugation 2 (->$C_{10}H_{17}N_3O_6S$). Results were filtered to minimize interference and background levels, specifically filtering for retention time (RT) greater than three minutes, mass shift less than 5 ppm and t_{120}/t_0 response ratio > 2 (Figure S-4).

Verified in FreeStyle version 1.6 (ThermoFisher Scientific, Waltham, MA, US.A), mass spectra and chromatographs of each potential metabolite were manually evaluated and confirmed if the *m/z* and RT matched at least two of three adduct ions present in the buffer ($[M + H]^+$, $[M + NH_4]^+$ and $[M + Na]^+$). The isotope mass distribution was also used to confirm identification. Peaks were averaged, background subtracted and the Gaussian 3 smoothing operator applied.

2.6 Quality Assurance and Control

The design of assay sets included one Wistar-Han rat biotransformation assay that consisted of three active replicates (containing NADPH), a method blank, TPHP positive control and two negative controls (NADPH-deficient and enzyme deactivated). Due to a limited amount of herring gull liver microsomes, two assays were conducted resulting in a total n=5 active replicates, n=4 NADPH-deficient controls, n=2 method blanks and n=2 enzyme-deactivated controls. Each active replicate contained 890 µL 2ppm (2.89 µM) BPADP standard buffer solution, 50 µL active Wistar-Han rat or herring gull microsomes, 50 µL NADPH A and 10 µL NADPH B. An identical procedure was applied to method blanks, which contained 790 µL deionized water and 100 µL pH 7.4 buffer rather than BPADP. NADPH-deficient controls contained 60 µL deionized water

rather than NADPH A and B while 50 µL microsomes denatured at 100 ^{o}C for 5 minutes replaced active microsomes in enzyme deactivated controls. TPHP positive controls consisted of 2 µL 60 ppm (183.88 µM) TPHP, 100 µL potassium phosphate pH 7.4 buffer and 788 µL deionized water rather than BPADP standard buffer solution. All test tubes were covered with aluminum foil throughout the assay to avoid evaporation and BPA contamination from plastic caps. For the initial target BPADP, BPA and DPHP metabolites, and ISs, Table S-4 details all UHPLC-QQQ-MS/MS instrument limits of detection and quantification (ILOD/ILOQ).

For target and non-target analyses, sample sets for UHPLC-Q-Exactive-HRMS/MS analysis consisted of a method blank, four replicates at the zero minute time point and four replicates at the 120- min time point. The blank sample incubation contained 1748 µL of 0.1 M Biotage potassium phosphate (pH 7.4) buffer while all replicates (t=0 and t=120) contained 1748 µL of 2 ppm sonicated BPADP solution. All samples contained 32 µL deionized water, 100 µL Wistar-Han rat liver microsomes, 100 µL NADPH A and 20 µL NADPH B.

2.7 Data analysis

The difference in BPADP concentration between t_0 and t_2 during the *in vitro* RLM kinetics assays was divided by two minutes to represent the initial rate of reaction (V_0). This was calculated for each dosing concentration, and further for additional time points (t_5, t_{10}). A Hanes-Woolf plot was used to investigate maximal rate of biotransformation (V_{max}) and the Michaelis rate constant (K_m), with further use of both Lineweaver-Burk and Eadie-Hofstee plots for confirmation.

For UHPLC-QQQ-MS/MS determined and quantified data of target BPADP, BPA and DPHP, all statistical analyses for the were conducted using GraphPad Prism v9.3.1 (GraphPad Software, San Diego, CA, USA). D'Agostino-Pearson normality tests assessed data distribution

compared to Gaussian, where sample size was too small for the D'Agostino-Pearson and Anderson-Darling tests the Kolmogorov-Smirnov test of normality was used. Non-linear one-phase decay/association least squares fit functions were then used to plot time-dependent BPADP depletion and formation of metabolites. The Brown-Forsythe test was applied to determine the equality of means, with significance set to a p-value of < 0.05. Depletion of BPADP and target metabolite formation at each time point was tested for level of significance when compared to t_0 using a one-way analysis of variance (ANOVA) and post-hoc Dunnett's multiple comparisons test.

3. Results and discussion

3.1 BPA and DPHP target in vitro metabolites of BPADP

Compared to TPHP, BPADP depletion was very slow within the 120 min of the biotransformation *in vitro* in the RLM and HGLM assays, likely due to the higher molecular mass and structural complexity. DPHP formation in all kinetics assays was insufficient for the calculation of V_{max} or K_m values using Hanes-Wolf, Lineweaver-Burk and Eadie-Hofstee plot methods, therefore dosing concentrations of 1780 ng/mL (ppb; or 2.57 µM) were used for all further RLM and herring gull liver microsomal biotransformation assays. In the positive RLM microsomal assays that contained NAPDH, TPHP was 94 ± 8.19% (n=3) depleted by the 20-minute time point (Figure 1) at a 1.53 µM t_0 concentration. Optimized RLM assays at 2.57 µM, containing NADPH, demonstrated a mean 44 ± 10 % (n=9) BPADP depletion and mean 20 ± 7.0 % (n=3) depletion in the absence of NADPH (Figure 2a). Both target metabolites BPA and DPHP were quantified as *in vitro* metabolites of BPADP in RLM assays, though the former only in NADPH-deficient control samples (Figure 2a). The percent conversion $\left(\frac{[total\ metabolite\ formed]}{[total\ BPADP\ depleted]} * 100\right)$ of BPADP to DPHP was 2.6 % in RLM assays containing

NADPH, with a 3.9 % conversion rate of BPADP to BPA in NADPH-deficient assays. Depletion of BPADP in active replicates was significant ($p < 0.05$) at t_{90} and t_{120} relative to t_0, with significant formation of both target metabolites found to be statistically significant ($p < 0.05$) relative to t_0 (BPA: t_{90}, t_{120}; DPHP: t_{20}, t_{40}. t_{60}, t_{90}, t_{120}). TPHP concentrations were quantified in all active microsomal, enzyme deactivated, and NADPH-deficient samples, remaining low throughout all assays and attributable to impurities in the BPADP standard. A 46 ± 12 % conversion of TPHP to DPHP was quantified in positive controls.

In vitro metabolism of BPADP to DPHP appears to be linked to mediation by both CYP450 enzymes and NADPH-independent enzymes, potentially paraoxonase (PON) enzymes and/or aryl esterases. In the active microsomal samples, quantification of a time-dependent increase in BPA formation *in vitro* may have occurred but the presence of CYP450 enzymes could have feasibly resulted in the Phase II conjugation of the hydroxyl groups of BPA, and thus depletion of BPA. Other studies have demonstrated this previously in *in vitro* assays using rat liver S9 fractions (Yoshihara et al., 2004; Ousji et al., 2020). Preliminary evidence suggests paraoxonase (PON) enzymes may play a major role in BPADP *in vitro* HLM metabolism, where six hydroxylated and O-dealkylated NADPH-independent metabolites of BPADP were identified (Alves et al., 2018). The findings of Alves et al. (2018) as well as the present study demonstrate NADPH-deficient controls are crucial to an experimental design when investigating BPADP metabolism. This contrasts with the current understanding that CYP-mediated metabolism is an important pathway for many legacy OPEs (Bekele et al., 2021; van den Eede et al., 2013), suggesting the involvement of different enzymes in the mediation of novel OPE metabolism.

Herring gull liver microsomal assays showed no significant BPADP depletion or target BPA and DPHP metabolite formation, with similar depletion in both active replicates and enzyme

deactivated controls (Figure 2b), suggesting involvement of both enzyme-mediated and abiotic hydrolysis. While BPA concentrations in all samples were indistinguishable from the background, DPHP concentrations were quantifiable both in active and NADPH-deficient samples. Higher background levels of TPHP were quantified in herring gull liver microsomal assays (Figure S-1), however the mean 19 % (n=2) depletion of TPHP cannot fully account for the formation of DPHP quantified. While rapid *in vitro* depletion of several legacy OPEs has been reported in herring gulls (Greaves et al., 2016), the present results illustrate BPADP depletion to be considerably slower than that of lower molecular mass and structural complexity.

3.2 Additional target and non-target metabolites in the in vitro assays

UHPLC-Q-Exactive-HRMS/MS analysis identified eight additional *in vitro* metabolites of BPADP, which included bisphenol A-(diphenyl phosphate) (BPA-DPP), bisphenol A-(diphenyl phosphate)-(monophenyl phosphate) (PBA-DPP-MPP), three BPADP+O metabolite isomers (X1, X2, X3), and two BPADP +2O metabolite isomers (X4, X5) (Table 1, Figure 3). These results were confirmed by a Compound Discoverer (CD) search via retention times, mass shifts, t_{120}/t_0 response ratios and full scan mass spectra (Table 1, Figure S-2). In full scan mass mode (HRMS), identification of these metabolites were depended on their *m/z* and isotope distribution. The results showed that the measured *m/z* and isotope distribution matched very well with the theoretical value (Figure S-2). Metabolites of BPA and DPHP were not confirmed by UHPLC-Q-Exactive-HRMS/MS) with ESI(-) analysis, likely due to low conversion rates and lower sensitivity of the UHPLC-Q-Exactive-HRMS/MS analysis compared to UHPLC-QQQ-MS/MS analysis.

Four of the addition metabolites identified by UHPLC-Q-Exactive-HRMS/MS analysis could be measured by UHPLC-QQQ-MS/MS with negligible response interferences, and where

each displayed clearly increasing peak area responses during the 0 to 20 min incubation time (Figure 3). However, quantitation was not possible due to lack of available chemical standards. The results described were by comparison of the *m/*z response level (representing the mass chromatographic peak area) at all time points relative to control samples. In both rat and gull assays, each oxidation metabolite demonstrated an increase in peak response over time which required NADPH, suggesting CYP450-mediated metabolism. BPA-DPP-MPP displayed a time-dependent increase in peak area in the presence and absence of NADPH and in both model species, while BPA–DPP was identified in rat only in the NADPH-deficient control but both in the presence and absence of NADPH in gulls. Alves et al. (2018) identified BPA–DPP via both enzymatic and non-enzymatic hydrolysis pathways and while abiotic hydrolysis of BPADP was not investigated in the present study, the findings also suggested BPA–DPP may be formed by both enzymatic (likely PON-mediated) and abiotic/chemical hydrolysis. While formation rates could not presently be calculated for these compounds, the identification of additional target BPADP metabolites increases the understanding of the array of degradation compounds that make up the total BPADP biotransformation mass balance. Corresponding to the much slower depletion rate of BPADP in gulls, the peak areas of each of the additional four target metabolites were lower for gull compared to rat assays.

A glutathione (GSH) adduct of BPADP was confirmed via mass spectra (Figure S-3) from UHPLC-Q-Exactive-HRMS/MS analysis and Compound Discoverer in the fraction from the *in vitro* assay with RLM (Table S-5). The posited structure in Table 1 is accurate as to the exact mass and molecular formula identified via UHPLC-Q-Exactive-HRMS/MS, however, the specific adduct location is unconfirmed and the possible structure presented here is based on recent study in our lab of TPHP-GSH adducts from an *o*-hydroquinone intermediate and reaction

with *o*-benzoquinone (Chu and Letcher, 2019). Glucuronidation and sulfation of the BPADP metabolites were previously identified in HLM S9 fraction incubated with BPADP, chemical formulas $C_{33}H_{33}O_{11}P$ and $C_{27}H_{25}O_8PS$, respectively (Alves et al., 2018). The present results are therefore the first report on the identification of a specific Phase II metabolite from BPADP GSH conjugation namely $C_{49}H_{49}N_3O_{16}P_2S$ (BPADP + GSH + 2O - 2H).

3.3 In silico metabolite predictions and physico-chemical property estimations

Rat liver S9 and microsomal *in silico* simulated metabolites of BPADP (Table 1) included the target metabolite DPHP, while BPA was simulated only as a rat *in vivo* metabolite. EPI Suite™ predicted physico-chemical properties varied widely from limited available experimental values (Table 2). Predicted logK_{OW} and logK_{OC} of BPADP were 10.02 and 6.24, respectively, both estimates being very high relative to well-studied compounds and suggesting overestimation of physicochemical properties due to the high molecular mass and low water solubility of BPADP. Greater than 4.5, the predicted logK_{OC} value suggests very high adsorption to and low mobility in sediment (US EPA, 2012) and possible deleterious effects to terrestrial ecosystems.

The combination of predicted high lipophilicity (or superhydrophobicity) and soil adsorption may indicate persistence and bioaccumulation of BPADP in sediment or terrestrial environments, however this may also limit contaminant availability in aquatic environments (Gobas et al., 2003). In both phytoplankton and zooplankton the OPEs tricresyl phosphate (TMPP), 2-ethylhexyl diphenyl phosphate (EHDPP), triphenyl phosphate (TPHP), tris(2-ethylhexyl) phosphate (TEHP) and tris(1,3-dichloro-2-propyl) phosphate (TDCIPP) were quantified and bioavailability between sediment and biota increased with hydrophobicity (Wang et al., 2019). Bioavailability was also found to plateau at logK_{OW} values >5.73 and was affected by

biotransformation rates of individual organisms at various trophic levels. High sediment concentrations of OPEs can contribute to aquatic species ingesting OPEs on a continuous basis, potentially leading to magnification up a trophic system depending on the properties of individual compounds (Yao et al., 2021). Additional experimentally derived physicochemical properties are needed, particularly a specific logK_{OW} value, in order to better understand the bioaccumulation and biomagnification potential of BPADP. Persistence and accumulation warrants further investigation given that all predicted or measured logK_{OW} values of BPADP exceed the threshold of 5, denoting potential of bioaccumulation, and the estimated persistence in sediment exceeds 365 days/12 months as per CEPA 1999 Persistence and Bioaccumulation Regulations (Environment Canada, 2004). BPADP lipophilicity may be similar to or exceed that of previously studied contaminants including polychlorinated biphenyl (PCB) and PBDE congeners (Table 2), which have demonstrated high bioconcentration and bioaccumulation potential. The environmental fate of BPADP possibly being similar would be highly relevant if production and usage increases in the future.

One metabolite (Supplier Name 'SCHEMBL12670502') was corroborated by all lines of evidence, i.e. predicted *in silico* and confirmed experimentally as an *in vitro* metabolite via UHPLC-MS/MS and Compound Discoverer, and is the first experimental identification of this BPADP metabolite. *In silico* profiling via the OECD Toolbox^{TM} also predicted the metabolites BPA-DPP-MPP, BPA and DPHP which were each confirmed *in vitro.* Despite being simulated only *in vivo*, BPA was confirmed *in vitro* in the present study. Simulated metabolites did not include any Phase I oxidation metabolites of Phase II conjugates, therefore predictions should be interpreted conservatively- particularly for novel OPEs such as BPADP for which literature data is scarce. Given the advantage of time saved, *in silico* modelling applications such as the OECD

Toolbox^{TM} could be useful in identifying novel OPEs for which metabolites may be of concern, and in identifying compounds of research priority. The present study being an *in vitro* investigation of BPADP biotransformation, additional *in vivo* metabolites are feasible as are *in vitro* S9 fraction and non-GSH Phase II *in vitro* conjugates.

3.4 Implications for the environmental fate of BPADP and risk assessment relevance

The slow metabolism, biotransformation and depletion of BPADP in the present study suggests the potential for environmental persistence and bioaccumulation, coupled with the low but quantifiable conversion to BPA, a well-established xenoestrogen (Badamasi et al., 2020) and aquatic toxicant (Wu and Seebacher, 2020). In the absence of specific experimentally derived physicochemical properties, bioaccumulation and biomagnification of BPADP and other novel OPEs remains poorly understood. Limited available literature suggests BPADP partitions to soil and potentially bioaccumulates (Zhao et al., 2019) illustrating the relevance of BPADP bioavailability to hazard and risk assessment. Low conversion rates of BPADP to target metabolites may result in chronic, low-dose exposure of BPA and DPHP to biota.

3. Conclusions

BPADP metabolism is presently shown to be slow in both the Wistar-Han rat (mammalian) and herring gull (avian) models. Both metabolites of BPA and DPHP were confirmed in the rat model, with eight additional metabolites identified and confirmed as *in vitro* metabolites of BPADP (BPA-DPP, BPA-DPP-MPP, BPADP+O, BPADP+2O, BPADP+GSH+2O-2H). *In silico* modelling proved to be a valuable prediction tool for BPADP metabolite formation although these predictions should be interpreted with caution, and a lines of evidence approach is preferable given the lack of available literature data for novel OPEs.

Scientific understanding as to the persistence, fate and biotransformation products of novel OPEs is limited amidst projected increases in consumption, highlighting a need for efficient study of these compounds. The present study suggests BPADP may be highly stable and potentially bioaccumulative in environmental media and biota, however species-specific differences in metabolism could lead to variation in metabolite formation across exposed species. The structural complexity of novel OPEs allows for varied and complex degradation products, which may pose additional persistence and/or toxicity concerns and may vary between species. Addressing these knowledge gaps can elucidate whether exposure of novel OPEs to biota may add to the burden of PBT contaminants in a similar fashion as the PBDEs that OPEs were developed to replace.

Associated Content

Further information on UHPLC-MS/MS parameters (all multiple reaction monitoring transitions, instrument limits of detection/quantification), molecular mass spectra and background triphenyl phosphate (TPHP) can be found online.

Author Information

Corresponding Author

*Phone: +1 613-998-6696; fax: +1 613-998-0458; e-mail: Robert.Letcher@ec.gc.ca

Notes

The authors declare no competing financial interest.

Acknowledgements

Funding for this project was provided by the National Science and Engineering Research Council (NSERC) CREATE-REACT Program (to S.M.H), by BizNGO of Clean Production Action through Carleton University (to R.J.L), and the Environment & Climate Change Canada Chemical Management Plan (CMP) (to R.J.L.).

References

Alves, A., Erratico, C., Lucattini, L., Cuykx, M., Ballesteros-Gómez, A., Leonards, P.E.G., Voorspoels, S., Covaci, A., 2018. Mass spectrometric identification of *in vitro*-generated metabolites of two emerging organophosphate flame retardants: V6 and BDP. Chemosphere 212, 1047–1057. doi: 10.1016/j.chemosphere.2018.08.142

Badamasi, I., Odong, R., Masembe, C., 2020. Threats posed by xenoestrogenic chemicals to the aquatic ecosystem, fish reproduction and humans: a review. African Journal of Aquatic Science, 45:3, 243-258, doi: 10.2989/16085914.2020.1746233

Bekele, T.G., Zhao, H., Yang, J., Chegan, R.G., Chen, J., Mekonen, S., Qadeer, A. 2021. A review of environmental occurrence, analysis, bioaccumulation, and toxicity of organophosphate esters. Environmental Science and Pollution Research (2021) 28, 49507–49528, doi: 10.1007/s11356-021-15861-8

Blum, A., Behl, M., Birnbaum, L.S., Diamond, M.L., Phillips, A., Singla, V., Sipes, N.S., Stapleton, H.M., Venier, M., 2019. Organophosphate Ester Flame Retardants: Are They a Regrettable Substitution for Polybrominated Diphenyl Ethers? Environmental Science & Technology Letters 6(11), 638–649. doi: 10.1021/acs.estlett.9b00582

Center for Disease Control Agency for Toxic Substances and Disease Registry. Unknown date. PCBs – Chemical and Physical Information. Washington, DC, USA. Available at: https://www.atsdr.cdc.gov/toxprofiles/tp17-c4.pdf

Chu, S., Letcher, R.J., 2015. Determination of organophosphate flame retardants and plasticizers in lipid-rich matrices using dispersive solid-phase extraction as a sample cleanup step and ultra-high performance liquid chromatography with atmospheric pressure chemical ionization mass spectrometry. Analytica Chimica Acta 885, 183–190. doi: 10.1016/j.aca.2015.05.024

Chu, S., Letcher, R.J., 2018. A mixed-mode chromatographic separation method for the analysis of dialkyl phosphates. Journal of Chromatography A 1535, 63–71. doi: 10.1016/j.chroma.2017.12.069

Chu, S., Letcher, R.J., 2019. *In vitro* metabolic activation of triphenyl phosphate leading to the formation of glutathione conjugates by rat liver microsomes. Chemosphere 237, 124474. doi: 10.1016/j.chemosphere.2019.124474

Draganov, D.I., La Du, B.N., 2004. Pharmacogenetics of paraoxonases: A brief review. Naunyn-Schmiedeberg's Archives of Pharmacology 369(1), 78–88. doi: 10.1007/s00210-003-0833-1

Environment Canada, 2004. Canadian Environmental Protection Act, 1999 Environmental Screening Assessment Report on Polybrominated Diphenyl Ethers (PBDEs) – Draft for Public Comments. Available at: https://www.ec.gc.ca/lcpe-cepa/documents/substances/pbde/pbde_draft-eng.pdf

Environment Canada, 2013. ARCHIVED- Environmental Screening Assessment Report on Polybrominated Diphenyl Ethers (PBDEs) – Draft for Public Comments. Available at: https://www.ec.gc.ca/lcpe-cepa/default.asp?lang=En&n=DF7DE982-1&offset=3&toc=hide

European Chemicals Agency (ECHA), 2011. (1-methylethylidene)di-4,1-phenylenetetraphenyl diphosphate- Registration Dossier; Physical & Chemical Properties. Helsinki, Finland. Available at: https://echa.europa.eu/registration-dossier/-/registered-dossier/6592/4/8/?documentUUID=dae1147a-fc9c-4818-905c-78b84a7265a1

European Commission Joint Research Centre, 2001. Diphenyl Ether, Pentabromo Derivative (Pentabromodiphenyl Ether). Belgium. Available at: https://echa.europa.eu/documents/10162/781ee1e9-6c90-467e-998b-8910ca2793e5

Gobas, F. A. P. C., Kelly, B. C., Arnot, J. A. Quantitative Structure Activity Relationships for Predicting the Bioaccumulation of POPs in Terrestrial Food-Webs. QSAR & Combinatorial Science 22, no. 3: 329–36. doi: 10.1002/qsar.200390022.

Greaves, A.K., Su, G., Letcher, R.J., 2016. Environmentally relevant organophosphate triesters in herring gulls: *In vitro* biotransformation and kinetics and diester metabolite formation using a hepatic microsomal assay. Toxicology and Applied Pharmacology 308, 59–65. doi: 10.1016/j.taap.2016.08.007

Gustafsson, K., Björk, M., Burreau, S., Gilek, M., 1999. Bioaccumulation kinetics of brominated flame retardants (polybrominated diphenyl ethers) in blue mussels (Mytilus edulis). Environmental Toxicology and Chemistry 18(6), 1218–1224. doi: 10.1002/etc.5620180621

Krowech, G., Hoover, S., Plummer, L., Sandy, M., Zeise, L., Solomon, G., 2016. Identifying chemical groups for biomonitoring. Environmental Health Perspectives 124, A219-A226. doi: 10.1289/EHP537

National Institute of Environmental Health Sciences, 2018. Flame Retardants. North Carolina, USA. Available at: https://www.niehs.nih.gov/health/topics/agents/flame_retardants/index.cfm.

513 Organisation for Economic Co-operation and Development, 2021. The OECD QSAR Toolbox.
514 Paris, France. Available at: https://www.oecd.org/chemicalsafety/risk-assessment/oecd-qsar-
515 toolbox.htm
516 Ousji, O., Ohlund, L., Sleno, L., 2020. Comprehensive *In Vitro* Metabolism Study of Bisphenol
517 A Using Liquid Chromatography-High Resolution Tandem Mass Spectrometry. Chemical
518 Research in Toxicology 33, 6, 1468-1477. doi: 10.1021/acs.chemrestox.0c00042
519 Rossi, M., Heine, L., 2007. The Green Screen for Safer Chemicals: Evaluating Flame Retardant
520 for TV Enclosures. Somerville, MA, USA. Available at:
521 https://www.bizngo.org/static/ee_images/uploads/resources/EvaluatingFlameRetardants_Gre
522 enScreenSaferChemicals_2007.pdf.
523 Rubin, B.S., 2011. Bisphenol A: An endocrine disruptor with widespread exposure and multiple
524 effects. The Journal of Steroid Biochemistry and Molecular Biology 127:27–34. doi:
525 10.1016/j.jsbmb.2011.05.002
526 Schlechtriem, C., Böhm, L., Bebon, R., Bruckert, H.-J., Düring, R.-A., 2017. Fish
527 bioconcentration studies with column-generated analyte concentrations of highly
528 hydrophobic organic chemicals. Environmental Toxicology and Chemistry 36(4), 906–916.
529 doi: 10.1002/etc.3635
530 Strobel, A., Willmore, W.G., Sonne, C., Dietz, R., Letcher, R.J., 2018. Organophosphate esters
531 in East Greenland polar bears and ringed seals: Adipose tissue concentrations and *in vitro*
532 depletion and metabolite formation. Chemosphere 196: 240–250. doi:
533 10.1016/j.chemosphere.2017.12.181
534 Su, G., Letcher, R.J., Yu, H., 2015. Determination of organophosphate diesters in urine samples
535 by a high-sensitivity method based on ultra high pressure liquid chromatography-triple

quadrupole-mass spectrometry. Journal of Chromatography A 1426, 154–160. doi: 10.1016/j.chroma.2015.11.018

United Nations Environment Programme, 2019. Stockholm Convention Polybromodiphenyl ethers—Overview. Chatelaine, Switzerland. Available at: http://chm.pops.int/Implementation/IndustrialPOPs/BDEs/Overview/tabid/5371/Default.aspx

United States Environmental Protection Agency, 2012. Estimation Programs Interface Suite™ for Microsoft® Windows, v 4.11. Washington, DC, USA

van der Veen, I., de Boer, J., 2012. Phosphorus flame retardants: Properties, production, environmental occurrence, toxicity and analysis. Chemosphere 88(10), 1119–1153. doi : 10.1016/j.chemosphere.2012.03.067

Van den Eede, N., Maho, W., Erratico, C., Neels, H., Covaci, A., 2013. First insights in the metabolism of phosphate flame retardants and plasticizers using human liver fractions. Toxicology Letters 223:9–15. doi: 10.1016/j.toxlet.2013.08.012

Velencoso, M.M., Battig, A., Markwart, J.C., Schartel, B., Wurm, F.R., 2018. Molecular Firefighting—How Modern Phosphorus Chemistry Can Help Solve the Challenge of Flame Retardancy. Angewandte Chemie International Edition 57(33), 10450–10467. doi: 10.1002/anie.201711735

Wang, X., Zhong, W., Xiao, B., Liu, Q., Yang, L., Covaci, A., Zhu, L., 2019. Bioavailability and biomagnification of organophosphate esters in the food web of Taihu Lake, China: Impacts of chemical properties and metabolism. Environment International 125, 25–32. doi: 10.1016/j.envint.2019.01.018

Wu, N., Seebacher, F., 2020. Effect of the plastic pollutant bisphenol-A on the biology of aquatic organisms: A meta-analysis. Global Change Biology 26: 3821–3833. doi: 10.1111/gcb.15127

Yao, C., Yang, H., Li, Y., 2021. A review on organophosphate flame retardants in the environment: Occurrence, accumulation, metabolism and toxicity. Science of the Total Environment 795, 148837. doi: 10.1016/j.scitotenv.2021.148837

Yoshihara, S., Mizutare, T., Makishima, M., Suzuki, N., Fujimoto, N., Igarashi, K., Ohta, S., 2004. Potent Estrogenic Metabolites of Bisphenol A and Bisphenol B Formed by Rat Liver S9 Fraction: Their Structures and Estrogenic Potency. Toxicological Sciences 78(1), 50–59. doi: 10.1093/toxsci/kfh047

Zhao, H., Liu, L., Li, Y., Zhao, F., Zhang, S., Mu, D., Liu, J., An, L., Wan, Y., Hu, J., 2019. Occurrence, Bioaccumulation, and Trophic Transfer of Oligomeric Organophosphorus Flame Retardants in an Aquatic Environment. Environmental Science & Technology Letters 6(6), 323–328. doi: 10.1021/acs.estlett.9b00262

Zhong, W., Cui, Y., Li, R., Yang, R., Li, Y., Zhu, L., 2021. Distribution and sources of ordinary monomeric and emerging oligomeric organophosphorus flame retardants in Haihe Basin, China. Science of the Total Environment 785, 147274. doi: 10.1016/j.scitotenv.2021.147274

Tables

Table 1. Comparison of the multiple lines of evidence of the metabolites of BPADP from *in vitro* biotransformation (targeted and NTA) and predicted *in silico* via OECD Toolbox v4.4.1 (*in vivo* and *in vivo* rat simulation).

Metabolite Chemical Formula	Abbreviation	*In silico*	*In vitro* target analysis	*In vitro* NTA	Posited Chemical Structure
$C_{27}H_{25}O_5P$	SCHEMBL811002; BPA-DPP	✓	✓	n/a	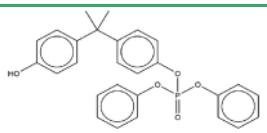
$C_{33}H_{30}O_8P_2$	SCHEMBL12670502; BPA-DPP-MPP	✓	✓	✓	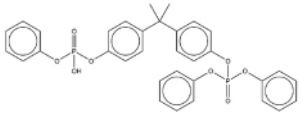
$C_{12}H_{11}O_4P$	diphenyl phosphate (DPHP)	✓	✓	x	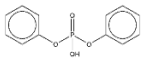
C_6H_6O	phenol	✓	n/a	x	
$C_{15}H_{16}O_2$	bisphenol A* (BPA)	✓	✓	x	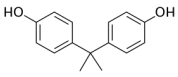
$C_{39}H_{34}O_9P_2$	BPADP + O (X1, X2, X3 isomers)	x	✓	✓	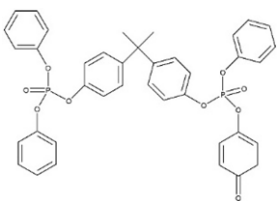

$C_{39}H_{34}O_{10}P_2$	BPADP + 2O (X4, X5 isomers)	x	✓	✓	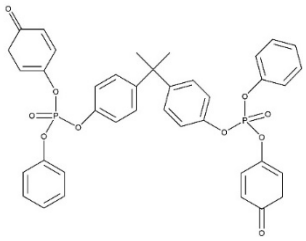
$C_{49}H_{49}N_3O_{16}P_2S$	BPADP+GSH+ 2O-2H	x	✓	✓	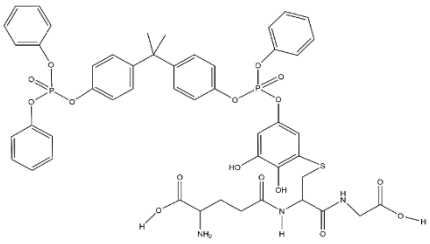

580

Table 2. EPI Suite™ predicted physico-chemical properties of bisphenol A bis(diphenyl phosphate) (BPADP), resorcinol diphenyl phosphate (RDP) and tetrakis(2,6-dimethylphenyl)-m-phenylene biphosphate (RDX). Comparison is made to available experimental values and legacy persistent, bioaccumulative and toxic (PBT) pollutants, bolded values exceed Canadian Environmental Protection Act (CEPA) guidelines.

	BPADP	**RDP**	**RDX**
Water Solubility (mg/L) WSKOWWIN™ *WATERNT*™ Experimental	1.09e-7 *1.88e^{-6}* 0.212* to 0.4*	1.11e^{-4} *6.88e^{-3}* 0.015*	3.70e^{-9} *6.87e^{-7}* n/a
Soil Adsorption Coefficient (logK_{OC}) (KOCWIN™) Experimental	10.52 4.00 ± 0.473; 4.76 ± 0.252	8.32	10.03
Octanol-Water Coefficient (logK_{OW}) (KOWWIN™) Experimental	10.02 ≥6	7.41	11.79
Octanol-Air Coefficient (logK_{OA}) (KOAWIN™)	21.74	18.33	22.37
Air-Water Coefficient (logK_{AW}) (HENRYWIN™)	-11.72	-10.92	-10.58
Vapour Pressure (MPBPVP™)	5.99e^{-10} to 5.61e^{-6}	5.99e^{-10} to 5.61e^{-6}	5.99e^{-10} to 5.61e^{-6}
Estimated Fugacity $t_{1/2}$ (hr) (LEV3EPI™) Air; Water; Soil; Sediment	10.94; 1440; 2880; 1.30e^{4}	12.13; 900; 1800; 8100	5.48; 4320; 8640; 3.89e^{4}

Comparison of BPADP to legacy PBT compounds

	BPADP	**PCB-153**	**tetraBDE** (congeners present in commercial PeBDE, OBDE and DBDE)	**pentaBDE** (2 congeners, specific nomenclature not disclosed)
logK_{OW}	8*	6.72, 8.35	6.81	6.64-6.97; 6.57
Molecular Weight (amu)	692.63	360.88	485.79	564.7
Bioconcentration Factor (BCF) (L/kg wet weight)	644.3*	1.8539e^{4}	1.3e^{6} ; 6.67e^{4}	2.74e^{4} ; 1.77e^{4} ; 1440
Bioaccumulation Factor (BAF) (L/kg wet weight)	1790*	2.1e^{5}	n/a	1.4e^{6}

*conservative estimate of BPADP logK_{OW} between experimental value and *in silico* predictions, used as an input value to predict BCF and BAF via EPI Suite™

Environment Canada, 2004, 2013; Gustafsson *et al.*, 1999; EU 2001; CDC ATSDR; Schlechtriem *et al.*, 2016 ; Zhong et al., 2021

Figure Legends

Figure 1. Comparison of the *in vitro* depletion of BPADP and the triphenyl phosphate (TPHP) positive control over a 60-minute incubation period in a rat liver microsomal assay. Each data point is the average of triplicate samples (n =3).

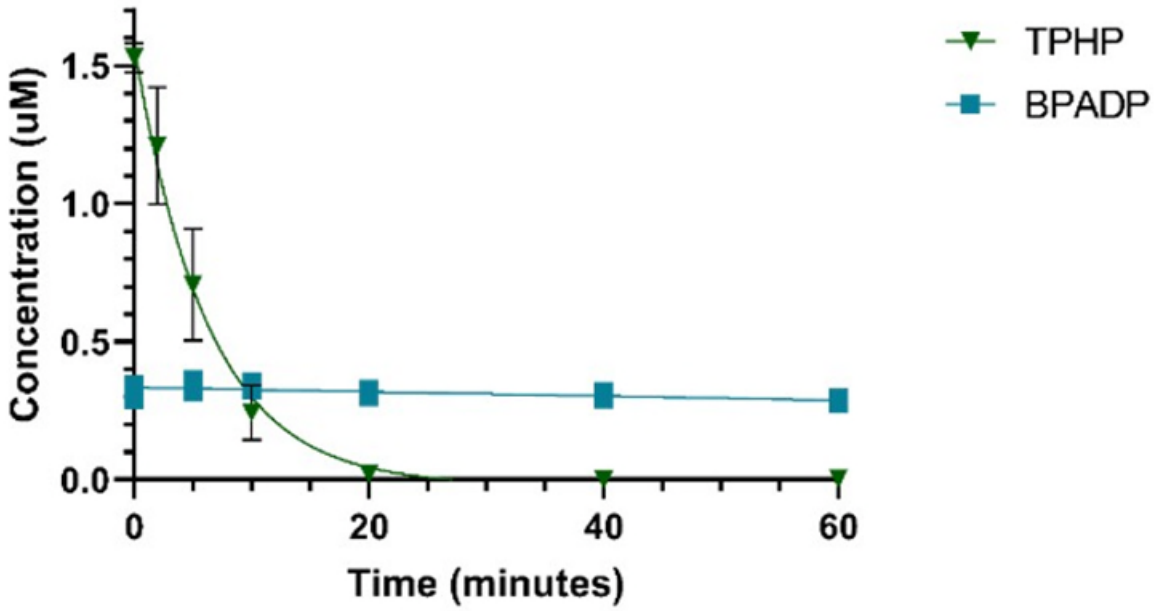

Figure 2. BPADP depletion and formation of the target metabolites diphenyl phosphate (DPHP) and bisphenol A (BPA) in assays of a 1780 ppb (2.57 µM) incubation concentration in both Wistar-Han rat (WH Rat) **(a)** and Great Lakes herring gull (HERG) **(b)** liver microsomal *in vitro* assays. Each herring gull active replicate data point is the mean of inter-day triplicate (n=3) and duplicate (n=2) assays (total n=5 replicates). Error bars represent the standard deviation of each mean and an asterisk represents a time point where the active microsomal concentration of BPADP or DPHP or the NADPH-deficient concentration of BPA differs significantly ($p < 0.05$) from that of zero minutes at the start of the assay.

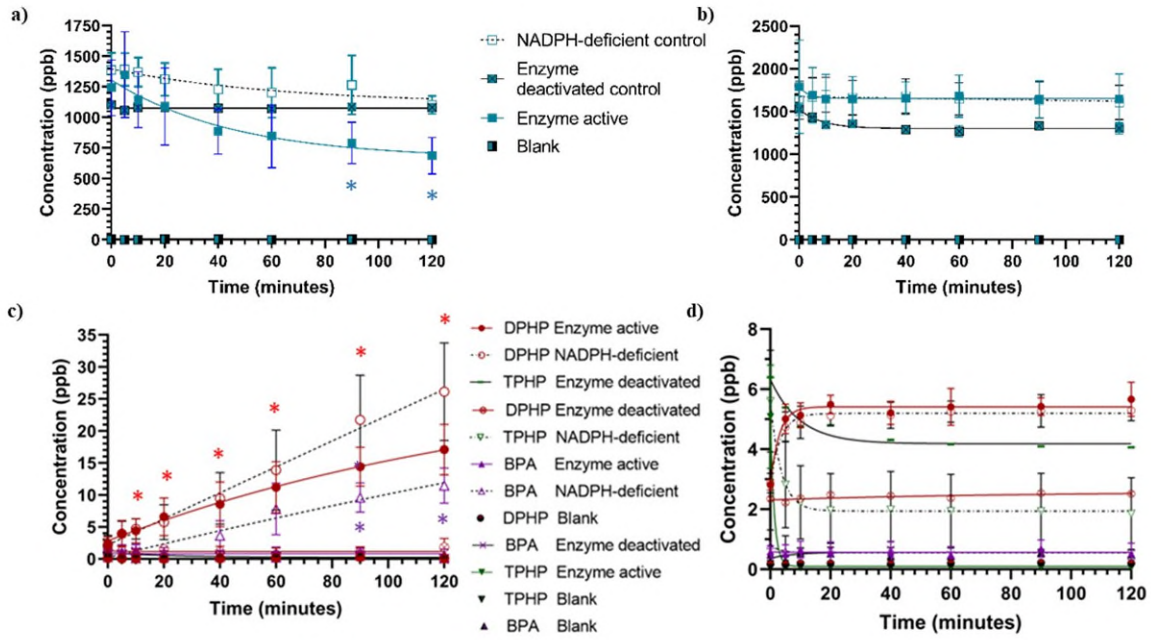

606 **Figure 3.** UHPLC-QQQ-MS/MS analysis response vs. incubation time for four additional
607 metabolites of BPADP: **(a)** BPADP + O (X2); **(b)** BPADP + 2O (X4); **(c)** BPA-DPP; **(d)** BPA–
608 DPP-MPP in Wistar-Han rat (WH Rat) and Great Lakes herring gull (HERG) liver microsome
609 assays. All data points are the mean of three replicates (n=3), error bars represent standard
610 deviation.
611

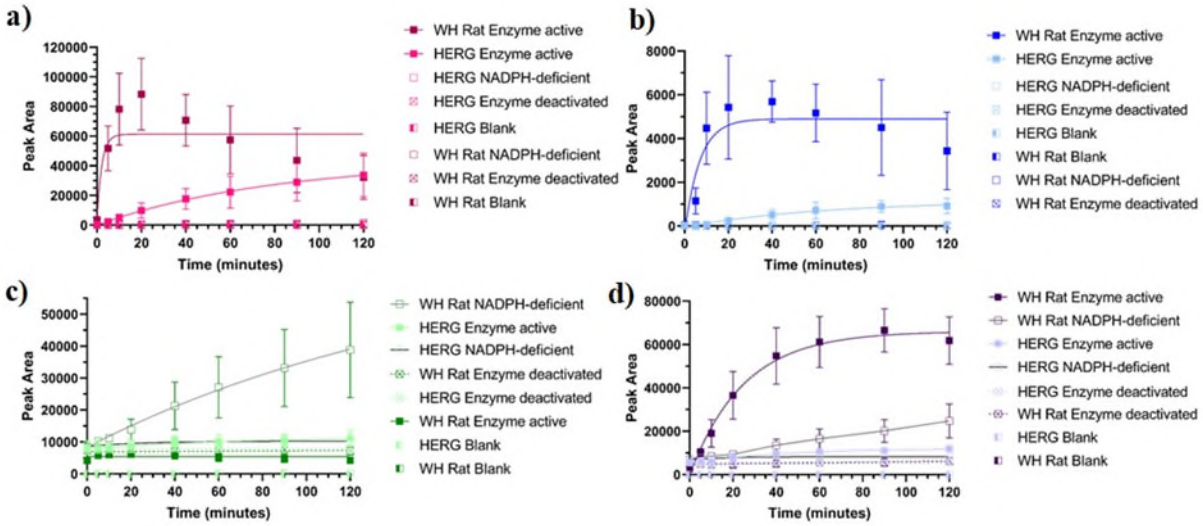

612
613
614

Supplementary Information

Biotransformation of bisphenol-A bis(diphenyl phosphate): *In vitro, in silico*, and (non-) target analysis for metabolites in rat and bird liver microsomal models

Sofia M. Herczegh[a,b], Shaogang Chu[a], Robert J. Letcher[a,b*]

[a] Ecotoxicology and Wildlife Health Division, Environment and Climate Change Canada, National Wildlife Research Centre, Carleton University, Ottawa, ON, K1A 0H3, Canada

[b] Department of Chemistry, Carleton University, Ottawa, ON, K1S 5B6, Canada

* Corresponding author: Robert J. Letcher; Phone: 1-613-998-6696; Fax: 1-613-998-0458; E-mail: robert.letcher@ec.gc.ca.

UHPLC-Q-Exactive-HRMS/MS analysis

Non-target analysis (NTA) for additional metabolites was via a Vanquish UHPLC coupled with a quadrupole orbitrap mass spectrometer (UHPLC-Q-Exactive-HRMS/MS; ThermoScientific, Waltham, MA, USA). The mobile phases were the same as that used in UHPLC-QQQ-MS/MS. A Kinetex XB-C18 column (100 x 2.1 mm, 1.7 µm particle size) was used for separation. The flow rate was 0.3 mL/min and the gradient elution ramping was 5 % B to 95 % B to 10 minutes, held for 10 minutes and after that the mobile phase composition was returned to initial conditions in 1 min and then equilibrated for 5 min. The UHPLC-Q-Exactive-HRMS/MS was operated in both full scan mode and data depended acquisition fragment analysis (dd-MS2/dd-SIM, DDA) mode. The MS was performed in positive polarity (ESI (+)) and negative polarity (ESI(-)) with 70 000 resolution, scanning over the range of 70 to 1050 *m/z*. Ion source parameters consisted of: 2.5 K spray voltage, S-lens RF level of 55, 45 sheath gas flow rate, 10 auxiliary gas flow rate and zero sweep gas flow rate, 350 °C desolvation capillary temperature, 450 °C aux gas heater temperature. Lock masses were 445.12003 *m/z* $(Si(CH_3)_2O))_6$ for positive mode and 255.23295 *m/z* ($C_{16}H_{32}O_2$) for negative mode. In full scan mode, AGC target was 10^6 and maximum IT is 200 ms. In dd-MS2/dd-SIM mode, the resolution is 17500; AGC target was 10^5; maximum IT was 50 ms; lop count was 5; isolation window was 1.2 *m/z*; NCE was 30.

For identification of GSH adducts via UHPLC-Q-Exactive-HRMS/MS, a Zorbax eclipse Plus C18 Rapid Resolution HT column (2.1 x 100 mm 1.8 µm particle size) was used. The column temperature was 40 °C and mobile phase flow rate was 0.3 mL/min. Mobile phase were water (A) and ACN (B) and both contained 0.1 % formic acid. The gradient started at 5 % B, held for 30 seconds before ramping up to 95 % B in 10 minutes, then held for 5 minutes,

659 decreased to 5 % B at minute 16, and then held until the end of the run at 21 minutes. MS was
660 performed in t-SIM mode with positive polarity (ESI(+)) to increase sensitivity, three most
661 possible target BPADP GSH adducts ions were selected in inclusion list, which included
662 BPADP+GSH-2H, BPADP+O+GSH and BPADP+O2+GSH-2H. The MS resolution was 70
663 000 and scanning range was 150 to 1200 *m/z* with a 4.5 *m/z* isolation window and AGC target
664 was $5e^4$ and maximum IT was 200 ms. Ion source parameters consisted of: 1.00 kV spray
665 voltage, S-lens RF level of 40.0, 80 sheath gas flow rate, 20 auxiliary gas flow rate and zero
666 sweep gas (N_2) flow rate, 300 °C desolvation capillary temperature, and 500 °C aux gas heater
667 temperature.

668

669 **Table S-1.** SMILES codes of all *in silico* OECD Toolbox v4.4.1 predicted metabolites of
670 BPADP (generated via *in vivo* rat simulation and rat liver *in vitro* S9/microsomal simulation) and
671 corresponding IUPAC Name, abbreviation and CAS RN.

Metabolite Identifier Label	Identified Compound
M1. SMILES code IUPAC Name/Abbreviation CAS RN	CC(C)(c1ccc(O)cc1)c1ccc(O)cc1; 4-[2-(4-hydroxyphenyl)propan-2-yl]phenol / bisphenol-A; 80-05-7
M2. SMILES code IUPAC Name/Abbreviation CAS RN	CC(C)(c1ccc(O)cc1)c1ccc(OP(=O)(Oc2ccccc2)Oc2ccccc2)cc1; [4-[2-(4-hydroxyphenyl)propan-2-yl]phenyl] phenyl hydrogen phosphate / SCHEMBL811002; n/a
M3. SMILES code IUPAC Name/Abbreviation CAS RN	CC(C)(c1ccc(O)cc1)c1ccc(OP(O)(=O)Oc2ccccc2)cc1; [4-[2-(4-hydroxyphenyl)propan-2-yl]phenyl] phenyl hydrogen phosphate / SCHEMBL2290182; n/a
M4. SMILES code IUPAC Name/Abbreviation CAS RN	CC(C)(c1ccc(OP(O)(=O)Oc2ccccc2)cc1)c1ccc(OP(=O)(Oc2ccccc2)Oc2ccccc2)cc1; [4-[2-[4-[Hydroxy(phenoxy)phosphoryl]oxyphenyl]propan-2-yl]phenyl] diphenyl phosphate / SCHEMBL12670502; n/a
M5. SMILES code IUPAC Name/Abbreviation CAS RN	CC(C)(c1ccc(OP(O)(=O)Oc2ccccc2)cc1)c1ccc(OP(O)(=O)Oc2ccccc2)cc1; [4-[2-[4-[Hydroxy(phenoxy)phosphoryl]oxyphenyl]propan-2-yl]phenyl] phenyl hydrogen phosphate / SCHEMBL3693240; n/a
M6. SMILES code IUPAC Name/Abbreviation CAS RN	CC(C)(c1ccc(OP(O)(O)=O)cc1)c1ccc(OP(=O)(Oc2ccccc2)Oc2ccccc2)cc1; n/a; n/a
M7. SMILES code IUPAC Name/Abbreviation CAS RN	OP(=O)(Oc1ccccc1)Oc1ccccc1; diphenyl hydrogen phosphate / diphenyl phosphate; 838-85-7
M8. SMILES code IUPAC Name/Abbreviation CAS RN	OP(O)(=O)Oc1ccccc1; phenyl dihydrogen phosphate / monophenyl phosphate; 701-64-4
M9. SMILES code IUPAC Name/Abbreviation CAS RN	Oc1ccc(O)cc1; benzene-1,4-diol / hydroquinone 123-31-9
M10. SMILES code IUPAC Name/Abbreviation CAS RN	Oc1ccccc1; phenol; 108-95-2
M11. SMILES code IUPAC Name/Abbreviation CAS RN	Oc1ccccc1O; 1,2-dihydroxybenzene / catechol; 120-80-9

672

673

Table S-2. Complete list of chemical reagents and compounds referenced, identified by CAS RN and including molecular weight and purity.

Reagent Name	**Molecular Weight (amu)**	**CAS #**	**Abbreviation**	**Supplier**	**Purity**
$^{13}C_{12}$-Bisphenol A	240.20	263261-65-0	$^{13}C_{12}$-BPA	Sigma-Aldrich	>98 %
Bisphenol A	228.29	80-05-7	BPA	Sigma-Aldrich	99+ %
Bisphenol A bis(diphenyl phosphate)	692.64	5945-33-5	BPADP	Toronto Research Chemicals	98 %
d_{10}-Diphenyl phosphate	260.25	1477494-97-5	d_{10}-DPHP	Toronto Research Chemicals	95 %
d_{15}-triphenyl phosphate	341.38	1173020-30-8	d_{15}-TPHP	Wellington Labs	>98 %
Diphenyl phosphate	250.19	838-85-7	DPHP	Sigma-Aldrich	99 %
Trans-1,4-cyclohexanediol-bis(diphenyl phosphate)	580.516	No CAS#	T-CH-BDP	Sigma-Aldrich	>97 %
Triphenyl phosphate	326.28	115-86-6	TPHP	Sigma-Aldrich	99+ %
L-Glutathione reduced	307.32	70-18-8	GSH	Sigma-Aldrich	≥98 %
Compound Name	**Molecular Weight (amu)**	**CAS #**	**Abbreviation**	**Supplier**	**Purity**
Phenol	94.11	108-95-2	n/a	n/a	n/a
Tetrakis(2,6-dimethylphenyl)-m-phenylene biphosphate	686	139189-30-3	RDX; PBDMPP	n/a	n/a
resorcinol bis (diphenylphosphate)	574.4	57583-54-7	RDP; PBDPP	n/a	n/a
Tetrakis(2-chloroethyl)dichloroisopentyldiphosphate	583	38051-10-4	V6; BCMP-BCEP	n/a	n/a

Table S-3. UHPLC-MS/MS analysis for determination of bisphenol A bis(diphenyl phosphate) (BPADP), targeted metabolites diphenyl phosphate (DPHP), triphenyl phosphate (TPHP), and bisphenol A (BPA), corresponding internal standards and additional targeted metabolites: functions, channels and compound-dependent operation parameters.

Function	Compound for Quantitative Analysis	Precursor ion (m/z)	Product ion(m/z)	Cone (v)	Coll. (v)	ESI	RT(min)	Internal Standard
1	TPHP	327.1	152.1	48	32	(+)	4.41	d_{15}-TPHP
		327.1	*77*	*48*	*36*			
	d_{15}-TPHP	342.2	160	48	32			
		342.2	*82*	*48*	*36*			
2	T-CH-BDP	581	251	42	18	(+)	4.95	
		581	*331.1*	*42*	*6*			
3	BPADP	693.2	367.1	80	38	(+)	5.45	T-CH-BDP
		693.2	*327.1*	*80*	*34*			
4	BPADP *	693.2	327.1	2	38	(+)	5.45	T-CH-BDP
		693.2	*367.1*	*2*	*34*			
5	BPA	227	133.1	52	26	(-)	3.45	$^{13}C_{12}$-BPA
		227	*212.1*	*52*	*12*			
	$^{13}C_{12}$-BPA	239	139.1	*52*	*26*	(-)	3.45	
		239	*224.1*	*52*	*12*			
6	DPHP	249	93.2	65	25	(-)	2.3	d_{10}-DPHP
		249	*155.1*	*65*	*20*			
	d_{10}-DPHP	259.1	98.2	65	25	(-)	2.26	
		259.1	*159.1*	*65*	*20*			
Function	Additional Compound	Precursor ion (m/z)	Product ion (m/z)	Cone (v)	Coll. (v)	ESI	RT(min)	
1	BPA-DPP	461.20	135.00	80	40	(+)	4.68	
		461.20	*327.10*	*80*	*40*			
2	BPA-DPP-MPP	617.1	327.1	80	40	(+)	4.27	
		617.1	*367.1*	*80*	*40*			
3	BPADP+O	709.2	327.1	80	40	(+)	5.10	
		709.2	*367.1*	*80*	*40*			
4	BPADP+2O	725.2	367.1	80	40	(+)	4.86	
		725.2	*465.2*	*80*	*40*			

* This function is for monitoring high concentrations of BPADP.
The italicized channels are for confirmation.

Table S-4. UHPLC-MS/MS limit of detection (ILOD) and limit of quantification (ILOQ) values for target compounds: bisphenol A bis(diphenyl phosphate) (BPADP), diphenyl phosphate (DPHP), triphenyl phosphate (TPHP) and bisphenol A (BPA).

#	Name	ILOD (ng/mL)	ILOQ (ng/mL)	Linearity-H (ng/mL)	Linearity-L (ng/mL)	r
1	TPHP	0.001	0.004		0-10	>0.99
3	BPADP	0.0008	0.003		0-10	>0.99
4	BPADP*	0.05	0.15	0-500		>0.99
5	BPA	0.09	0.29	0-500	0-500	>0.99
6	DPHP	0.01	0.04	0-500	0-500	>0.99

Table S-5. Chemical formula, parent compound, transformations, composition change (from parent compound), Δ mass shift, molecular weight, retention time (RT) and replicated group areas of the identified GSH adduct obtained from Q-Exactive HRMS (ThermoFisher Freestyle version 1.6 software).

Chemical Formula	**1: $C_{49}H_{49}N_3O_{16}P_2S$**
Parent Compound	Bisphenol A bis(diphenyl phosphate)
Transformations	Oxidation, Oxidation, GSH Conjugation 1
Composition Change	$+C_{10}\ H_{15}\ N_3\ O_8\ S$
Δ mass shift (ppm)	0.33
Molecular Weight (amu)	1029.23122
RT (min)	7.241
Replicated Group Areas (t_{120})	Replicate 1: $1.3e^5$; Replicate 2: $3.95e^4$; Replicate 3: $0.0e^0$; Replicate 4: $4.99e^5$

709

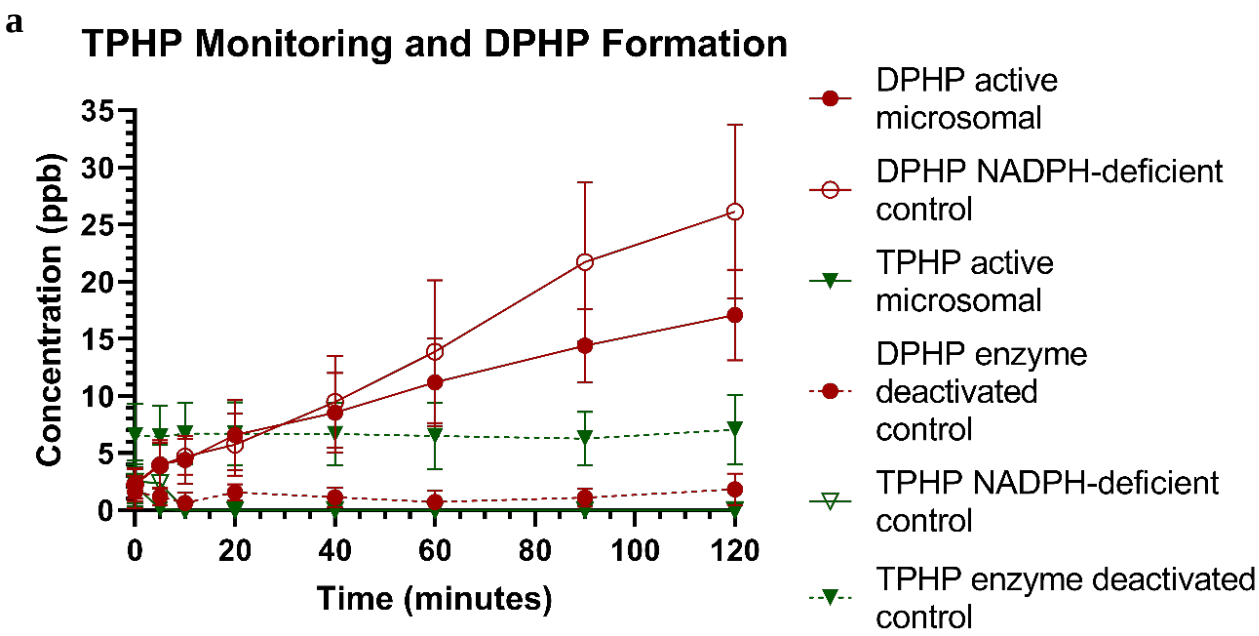

710

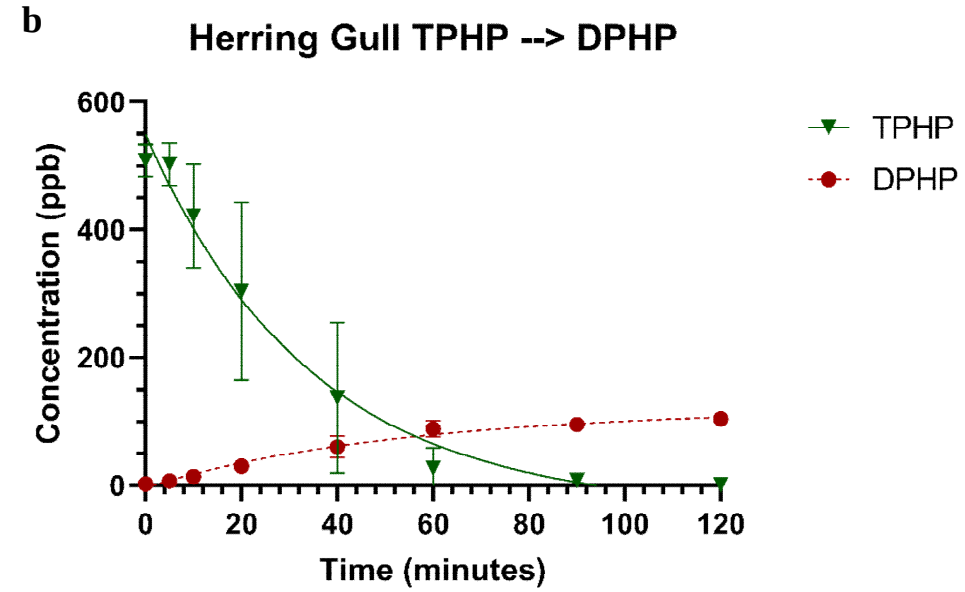

711 **Figure S-1. (a)** Mean TPHP and DPHP concentrations in each active replicate sample, NADPH-
712 deficient control and enzyme deactivated control of the assays conducted at a 1780 ppb BPADP
713 incubation concentration as presented in **Figure 2**. Each active microsomal data point is the
714 mean of three triplicate samples (n=9), each control data point is the mean of triplicate samples
715 (n=3). **(b)** Mean (n=2) TPHP depletion versus DPHP formation in Great Lakes Herring Gull
716 positive control samples.

717

718

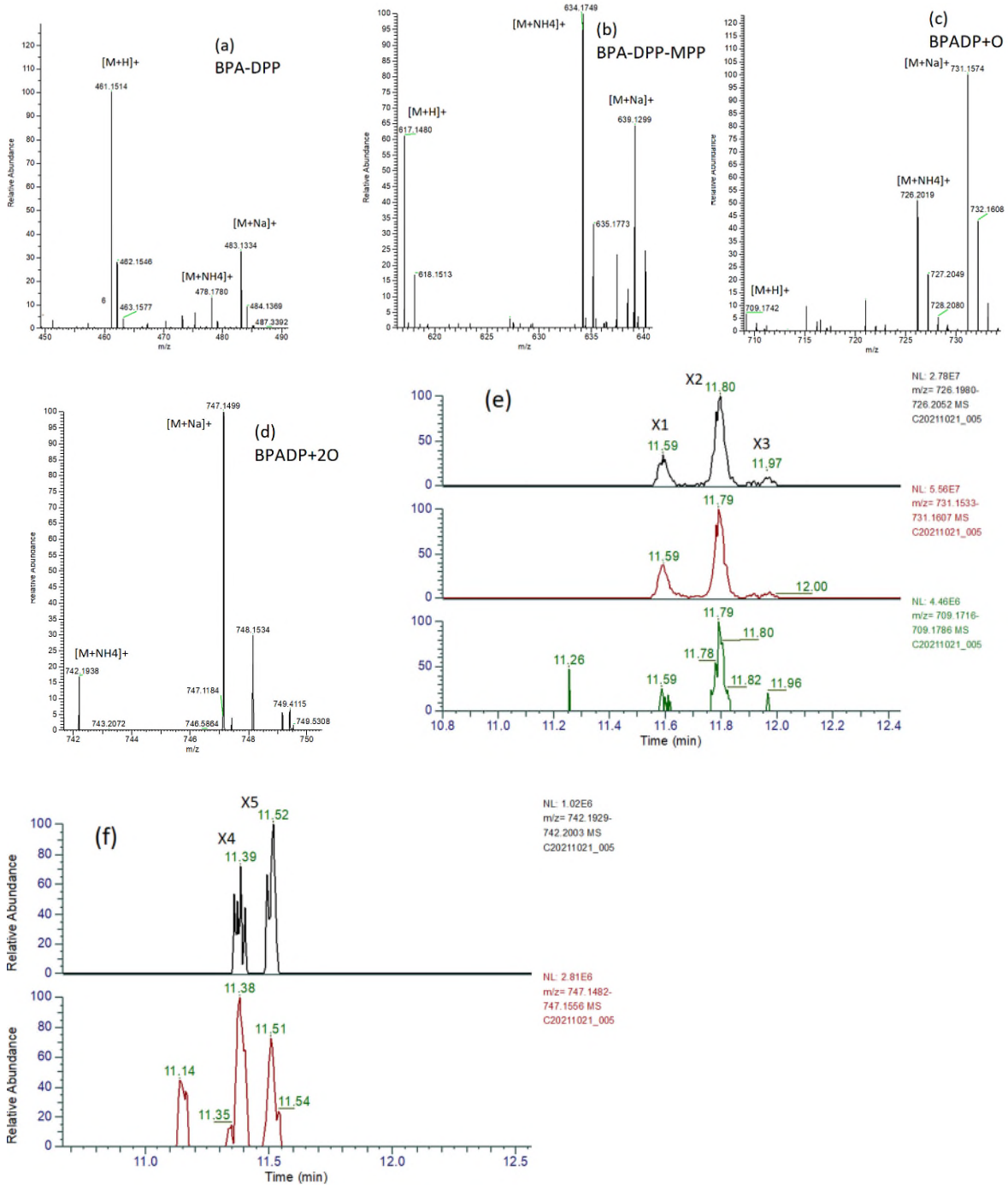

Figure S-2. Full scan mass spectra of confirmed metabolites of bisphenol A bis(diphenyl phosphate) (BPADP) identified via QE-Orbitrap and Compound Discoverer v3.2: (**a**) BPA-DPP; (**b**) BPA-DPP-MPP; (**c**) BPADP+O (X2) ; (**d**) BPADP+2O (X4); (**e**) Extracted ion chromatograms of BPA+O (*m/z* = 709.175, 726.202, 731.157); (**f**) Extracted ion chromatograms of BPA+2O (*m/z* = 742.197, 747.152)

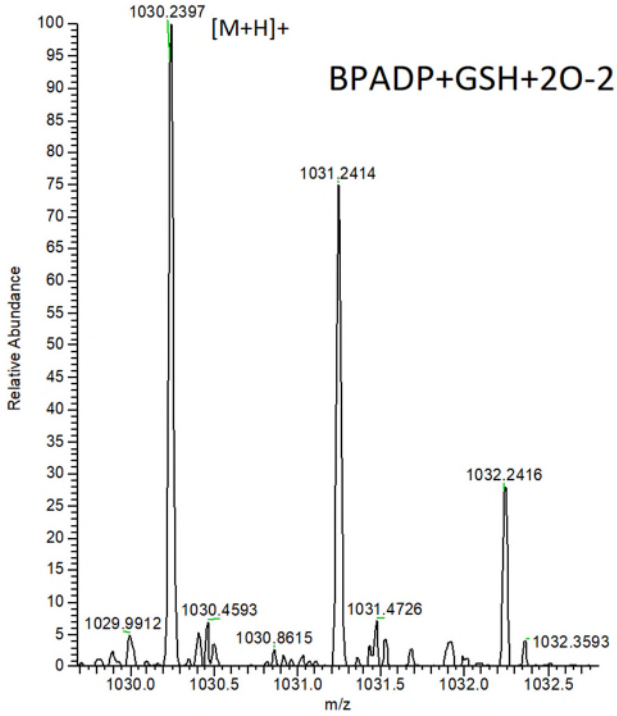

730

731 **Figure S-3.** Molecular mass spectra of the confirmed glutathione (GSH) adduct of BPADP:
732 BPADP+GSH+2O-2H.

733

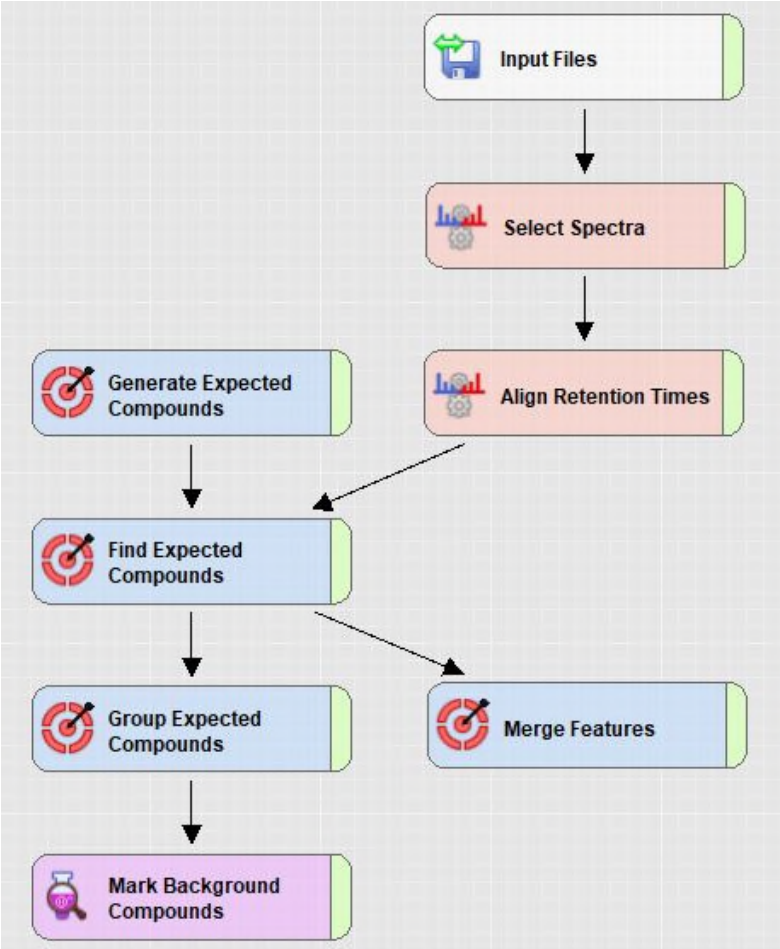

Figure S-4. Compound Discoverer v3.2 workflow tree developed for bisphenol A bis(diphenyl phosphate (BPADP) metabolite Non-Target Analysis (NTA).